Variability of the South Atlantic Convergence Zone Simulated by an Atmospheric General Circulation Model

MARCELO BARREIRO AND PING CHANG

Department of Oceanography, Texas A&M University, College Station, Texas

R. SARAVANAN

National Center for Atmospheric Research, Boulder, Colorado

(Manuscript received 21 February 2001, in final form 3 September 2001)

ABSTRACT

Interannual and decadal variability of the South Atlantic convergence zone (SACZ) during austral summer [season January–February–March (JFM)] is investigated. An attempt is made to separate the forced variability from the internal variability. This is accomplished by applying a signal-to-noise optimization procedure to an ensemble of multidecadal integrations of the latest version of the NCAR Community Climate Model (CCM3) forced with observed SST. The result yields two dominant forced atmospheric responses: a local response to Atlantic SST anomalies with interannual-decadal timescales and a remote response to Pacific SST anomalies at interannual timescales. The former is localized within the South Atlantic Ocean with almost no signal over land, consisting of a dipolelike structure in precipitation close to the coast of South America accompanied by a clockwise anomalous circulation of surface winds. The latter manifests itself mainly in the upper-level circulation, consisting of a northeastward shift of the SACZ with associated rainfall anomalies during warm ENSO events.

1. Introduction

The South Atlantic convergence zone (SACZ) is a band of convective activity with high rainfall rates that develops in a region defined roughly by (20°–40°S, 50°–20°W) in a northwest–southeast line. It extends from the active convective area in the Amazon to the southeast subtropical and extratropical Atlantic Ocean (Kodama 1992). The SACZ exists throughout the year, but has its largest manifestation in the summer [January–February–March (JFM)] of the Southern Hemisphere (SH).

Kodama (1992, 1993) suggested that the SACZ as well as other subtropical convergence zones, such as the South Pacific convergence zone (SPCZ), appear when two necessary conditions in the midlatitude circulation are satisfied: 1) subtropical jet flows in the subtropical latitudes (30°–35°S), and 2) low-level poleward flows prevail along the western peripheries of the subtropical highs. If these conditions are not satisfied, the convergence zone is weak and low rainfall rates are expected. This is because a poleward flow intensifies moisture convergence, and together with the subtropical jet they lead to favorable conditions for development of frontogenesis and convective instability. These conditions are usually met in the summer season together with the development of a heat low on the continent that increases the poleward flow in the eastern side of the continent, thus increasing moisture availability.

Corresponding author address: Dr. R. Saravanan, NCAR, P.O.Box 3000, Boulder, CO 80307-3000.
E-mail: svn@ncar.ucar.edu

Figueroa et al. (1995) reported the results of a regional eta-coordinate model simulation of the SACZ. Their results show that diabatic heating over the Amazon and the steep Andean topography are essential ingredients for the formation of the SACZ, while the inclusion of the climatological flow introduces modifications mainly in the location of the convergence zone. Lenters and Cook (1995), on the other hand, attribute the formation of the SACZ to the ''continentality,'' that is, the land–sea contrast in the absence of topography and longitudinal SST variations. Using a simple tropical atmosphere model, Wang and Li (1993) studied the formation of the SPCZ and suggested that the horizontal sea surface temperature (SST) gradients could originate this convergence zone. In the SACZ case, Figueroa et al. (1995) argue that warm SST does not play a very important role in the generation of the SACZ because the warm SST tongue in the South Atlantic does not coincide with the location of the SACZ, but lies to the north (as will be seen in Fig. 1). However, this does not necessarily exclude the possible influence of SST anomalies on the variability of the SACZ. In fact, the work of Lenters and Cook (1995), where the inclusion of nonzonal SST affected both the position and intensity of the SACZ, hinted the potential importance of SST influence.

In an observational and mechanistic study, Kalnay et al. (1986) reported the existence of a relationship between the strengthening of the SACZ and a strong eastward-shifted SPCZ in the Southern Hemisphere summer. They further speculate that this teleconnection would take place through changes in the Walker circulation during warm El Niño–Southern Oscillation (ENSO) years. In a more recent work, Robertson and Mechoso (2000) found that the SACZ shows both interannual and interdecadal variability. On interannual timescales, an intensification of the SACZ and associated anomalous descent to the southwest, are accompanied by an upper-troposphere cyclonic eddy in the lee side of the Andes. Accompanying these interannual variations are atmospherically forced SST anomalies with a dipolelike structure with a nodal line near 40°S. In their study interannual variability was found to be largely independent of ENSO. On interdecadal timescales, a 15–17-yr component was detected, which shows correlation to SST in the subtropical South Atlantic.

The purpose of this work is to examine the forced interannual and decadal variability of the SACZ. We are particularly interested in the forced part of the total variability because it is the only part that may have some predictability by knowing the changes in the boundary conditions beyond the 2-week limit of weather prediction imposed by the chaotic nature of the atmosphere. We hypothesize two possible ways that variability of the SACZ may be influenced by SSTs. The first would be a remote influence in which the ENSO-related variability in the tropical Pacific modifies the atmospheric circulation in the subtropical Atlantic leading to changes in precipitation. The second way is through the local influence of the Atlantic SST anomalies. A possible mechanism in the latter case, though not fully tested here, is that SST anomalies modify the stability properties of the atmospheric boundary layer producing changes in the convective activity and subsequently in the strength of the SACZ.

The paper is organized as follows. Section 2 introduces the model and datasets and describes the methodology used in this work. A comparison between simulated and observational climatologies and variabilities is given in section 3. In section 4 we investigate the preferred modes of variability in the SACZ region and search for forced responses using the signal-to-noise optimization procedure. Section 5 summarizes our findings and discusses their relationship with previous works.

2. Data and methodology

a. Data

The dataset used in this work consists of monthly mean fields from five runs of the latest version of the Community Climate Model (CCM3) developed at the National Center of Atmospheric Research (NCAR). The model has a spectral truncation T42 in the horizontal direction and 18 vertical levels. The five runs were forced with identical observed global SST from January 1950 to December 1994, but initialized with slightly different initial conditions in order to represent the internal atmospheric variability that has been shown to be fairly well reproduced by this model (Saravanan 1998). This set of runs has been referred to as the Global Ocean Global Atmosphere (GOGA) runs (e.g., Saravanan and Chang 2000). The specification of SST does not allow for any kind of feedback between the ocean and the atmosphere in the model. Since we are mainly interested in the SACZ variability, the analyses presented below are confined in the domain from 50°S to 20°N in latitude and from 70°W to 20°E in longitude. We analyze the variability only in the austral summer season, that is, JFM, since this is the season when the SACZ shows its mature development. Therefore, we take a seasonal average of the monthly mean data over these 3 months, which leaves us with an ensemble of 5 runs, each composed of 45 austral summers with a spatial resolution of roughly $2.8° \times 2.8°$ degrees.

Two key variables are chosen to describe the state of the simulated SACZ: the precipitation field as a measure of atmospheric convective activity, and the divergence of the upper-level (200 mb) winds as an indication of changes in the upper-level circulation of the atmosphere. To compare with observed variability, we use the Xie–Arkin dataset for the precipitation and the reanalysis dataset from the National Centers for Environmental Prediction (NCEP) for the upper-level wind flow. Both fields have been proven useful for characterizing large-scale, low-frequency variability of the SACZ (e.g., Robertson and Mechoso 2000). Since the observed and simulated datasets cover different time periods, the comparison of observed and modeled climatology and variability was made in the common time periods, that is, 1979–94 for precipitation and 1958–94 for the upper-level wind divergence.

b. Methodology

Finding a forced signal, either local or remote, in the subtropical atmosphere is not a trivial task due to the large atmospheric internal variability (Venzke et al. 1999; Chang et al. 2000). If we consider the internal variability as ''noise,'' this problem can be overcome by applying a so called signal-to-noise (S/N) optimization procedure (Allen and Smith 1997) to an ensemble of atmospheric GCM integrations (Venzke et al. 1999; Chang et al. 2000). Conceptually, this analysis is based on a prewhitening technique commonly used in signal processing. It is related to the optimal fingerprint algorithm of Hasselman (1979). We apply this S/N optimization analysis to extract the forced signal in the SACZ variability in much the same way as done in

Venzke et al. (1999) and Chang et al. (2000). Since this technique has already been described in detail in Venzke et al. (1999) and Chang et al. (2000), we will omit a lengthy description of the method. The interested reader is referred to these papers. Here, we will merely touch upon what lies at the heart of the algorithm: the prewhitening filter.

The prewhitening filter technique requires the construction of a filter based on the empirical orthogonal functions (EOF) calculated for the noise (internal variability only), which can be computed from the departures of each ensemble member from the ensemble mean. Results may depend on the number of EOFs, that is, truncation level, used to construct the filter. Usual values range from 15 (Venzke et al. 1999) to 36 (Chang et al. 2000). Chang et al. (2000) found that individual seasons show some sensitivity to the truncation level. Accordingly, sensitivity tests are needed to obtain robust results. In this study we found that results are stable when truncation level varies between 30 and 60 noise EOFs. Therefore, all the filters were constructed using 40 noise EOFs and the results shown below were based on this choice of truncation. This truncation level is in agreement with the rule of thumb discussed in Chang et al. (2000) in which a minimum number of five samples per truncation level is demanded.

Before applying the S/N optimization algorithm, we performed a conventional EOF analysis on the precipitation and upper-level wind divergence fields in order to find the dominant patterns of circulation in the atmosphere. Since these EOFs contain not only the forced response, but also the internal variability, we expect to find differences in the patterns obtained from different ensemble members. Two limiting cases are of interest: In the case where the forced signal is dominant, conventional EOFs and S/N optimals should be very similar in the sense that both patterns would be attributed to SST forcing, and associated time series should be significantly correlated to SST time evolution. In the case where the atmospheric internal variability dominates, conventional EOFs should show little connection to sea surface temperature anomaly. In the SACZ region, we expect the latter case to hold, that is, conventional EOFs and S/N optimals are likely to be different.

In addition to EOF analysis, correlation and regression analyses were also carried out in order to find relationships between sea surface temperature anomalies and atmospheric response. A Student's t-test was used to assess the local statistical significance of the correlations at the 95% significance level under the assumption that summer seasons in different years are independent (no year-to-year persistence) so that the number of degrees of freedom is equal to the number of data points. Values below the 95% significance level ($|r| < 0.3$) were considered to be not significantly correlated.

3. Climatology

The climatology and rms variability of the ensemble mean and of ensemble members are compared against observational counterparts. The rms of the ensemble members is calculated after concatenating all 5 members to form only 1 time series. We expect climatologies of ensemble mean and of ensemble members to be almost identical, but the rms of the ensemble mean to be significantly smaller due to the reduction of internal variability. If the model was perfect, then reality would be one realization of the ensemble runs. In this case we would expect that the observed data had the same statistics as the ensemble members. Therefore, the rms deviation of the observations should be compared to the rms deviation of ensemble members rather than that of the ensemble mean.

Figure 1 shows the climatology and rms deviation of the precipitation field for the ensemble mean, ensemble members and the Xie–Arkin data. Superimposed is the summertime climatology of the Atlantic SST. It is clear that the CCM3 reproduces the overall pattern of austral summertime precipitation. The SACZ appears as a northwest–southeast band of heavy precipitation off the coast of southern Brazil. The mean axis of maximum precipitation in the SACZ region is shown as a dashed line in Fig. 1a. The intensity of the SACZ is somewhat overestimated compared to the observations in much the same way as in the ITCZ region (Figs. 1a, 1c, and 1e). For comparison, in the Pacific sector the ITCZ and SPCZ regions are also somewhat overestimated, while in the monsoon trough the precipitation is not as large as in the observations. Note also that contrary to observations, the mean modeled ITCZ axis in the Atlantic sector is located to the south of the equator. The SACZ variability is indicated by the rms deviation maps (Figs. 1b, 1d, and 1f), which shows interannual variability of comparable magnitude as the seasonal means. As expected, although the patterns of rms deviation look similar in all three cases, the rms of ensemble members is in a closer agreement in magnitude with observations than that of the ensemble mean. A comparison between the rms variability of the ensemble mean and ensemble members indicates a significant reduction of the rms variability over South America for the ensemble mean, whereas the reduction over the ocean is much smaller. This suggests that the precipitation variability over the land is largely dominated by the internal variability of the atmosphere. Over the ocean the precipitation variability is more influenced by the surface boundary conditions, that is, SST.

To further quantify this assertion, we calculate the percentage of precipitation variability due to internal dynamics as given by the difference between the variability of ensemble members and that of the ensemble mean over the variability of ensemble members. The result indicates that over land approximately 65% of the total precipitation variance may be attributed to internal variability. Over the tropical Atlantic Ocean, ITCZ region, internal variability accounts only for 20% of precipitation variance, while in the subtropical regions of the Atlantic it accounts for 50% of total variance. In

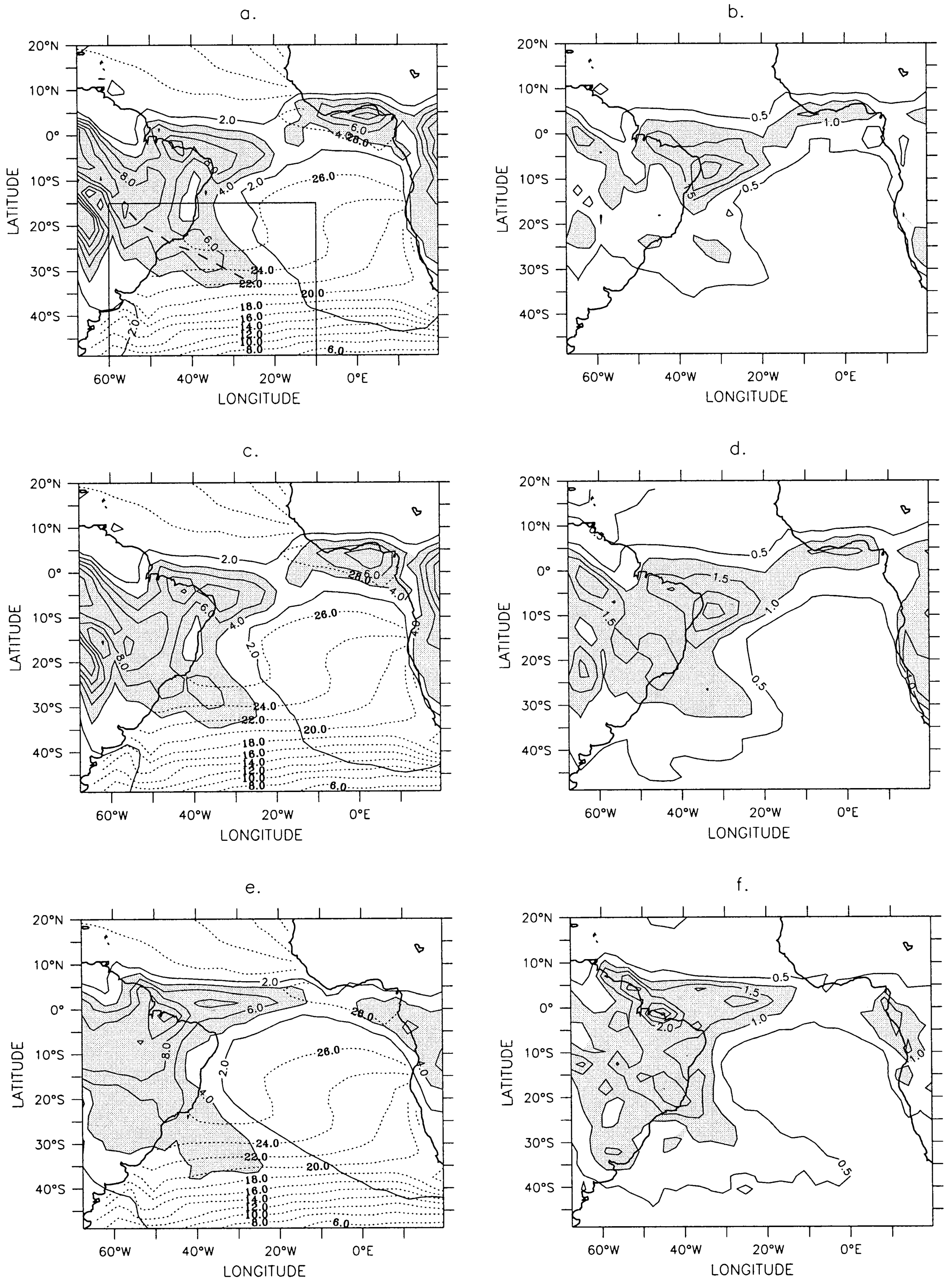

FIG. 1. (left) JFM precipitation climatology and (right) rms variability for period 1979–94 for (a), (b) CCM3 ensemble mean, (c), (d) CCM3 ensemble members, and (e), (f) Xie–Arkin dataset. Contour interval is 2 mm day^{-1} for climatologies and regions with more than 4 mm day^{-1} are shaded. Contour interval is 0.5 mm day^{-1} for rms maps. Superposed in climatologies is the observed mean SST for season JFM in °C (dotted lines). The box marks the SACZ region used for EOF analysis and the dashed line marks the mean precipitation axis in the SACZ region.

the SACZ region indicated by the rectangular box in Fig. 1, the mean explained precipitation variance by internal variability is 59%. Of particular interest is a relatively small area of the precipitation anomaly associated with the SACZ over the South Atlantic Ocean, where the internal variability explains only about 30% of total variance. The analysis presented below suggests that a significant portion of this precipitation anomaly can be explained as a forced response to South Atlantic SSTs.

Figure 2 shows the climatologies and rms variability of the 200-mb wind divergence in season JFM. The axis of mean maximum divergence in the SACZ region is shown as a dashed line in Fig. 2a. Here we contrast the CCM3 results with the divergence calculated from the NCEP reanalysis dataset. It is evident that the overall structures of the two climatologies bear certain resemblances. However, the SACZ in the CCM3 is more sharply defined and more closely connected to the convective activities over the Amazon basin and the ITCZ region than that in the NCEP reanalysis. The SACZ in the NCEP reanalysis has a particularly weak structure over the ocean (Figs. 2a, 2c, and 2e). This is in contrast to the ITCZ where the NCEP climatology shows a stronger structure than the CCM3. In terms of rms variability (Figs. 2b, 2d, and 2f), the SACZ structure is not as well defined as in the precipitation field, although a clear signal can still be identified in all three cases. Again, we find that the rms variability of the ensemble members bears closer resemblance in both spatial structure and magnitude to that of the NCEP reanalysis. Comparing Figs. 2b, 2d, and 2f, it is seen that the rms variability of the ensemble mean is significantly weaker than that of the ensemble members and of the NCEP reanalysis throughout the tropical Atlantic sector, suggesting that much of variability of the upper atmosphere is governed by the internal atmospheric variability.

In summary, we can conclude that the CCM3 reproduces reasonable well the climatology and rms variability of the precipitation and 200-mb wind divergence over the tropical and subtropical South Atlantic. It has been shown by many investigators (e.g., Hess et al. 1993), that different convective parameterizations may lead to different results in precipitation variability. Therefore, although the CCM3 appears to reproduce the major features of the SACZ fairly realistically, results may be, however, model dependent. An intercomparison study with other models and with higher resolution are desirable in the future in order to assure that results presented below are not resolution or model dependent.

4. Identification of forced responses

In this section we further analyze the precipitation and divergence fields using a number of statistical techniques to search for forced patterns of variability in the subtropical atmosphere. First, we applied conventional EOF and regression analyses to the simulations and compare the results with the corresponding observations. Then we employ the signal-to-noise optimization analysis to identify the forced response of the atmosphere to SST anomalies. All the analyses were performed in the region between 50° and 15°S in latitude and between 60° and 10°W in longitude (the box indicated in Fig. 1a). This choice of the analysis domain is made to isolate the variability of the SACZ from other stronger features of the climate system, such as the ITCZ.

Three indices were constructed to represent the possible SST forcings both from the tropical Pacific and Atlantic onto the atmosphere. The influence of ENSO is represented by the Niño-3 index defined as the average of SST anomalies over 5°S–5°N and 150°–90°W. To characterize the South Atlantic SST forcing, we used the principal components (PCs) of the two leading EOF modes of the SST anomaly, as shown in Fig. 3. The two leading EOFs account for 37% and 23% of the total variance, respectively. The first EOF shows a dipolelike pattern of SST anomalies, whereas the second shows a monopole centered at (30°S, 25°W). We use AT1 and AT2 to denote the PCs associated with the first two leading SST EOFs. Figures 3c and 3d show AT1 and AT2 (solid lines) along with Niño-3 index (dotted line) time series. The three time series show little correlation among each other. It is important to note that AT1 exhibits interannual timescales before the mid-1970s and decadal timescales after that, while AT2 is mostly dominated by interannual variability superimposed on a linear trend. The first SST EOF (Fig. 3a) resembles the second annual EOF of the South Atlantic SST obtained by Venegas et al. (1997).

a. Precipitation variability

EOFs were calculated using the covariance matrix of concatenated ensemble member anomalies. Figures 4a,b show the first and second leading EOFs of the precipitation field, which explain 23% and 18% of total variance, respectively. These EOFs are statistically distinct according to the rule of thumb given by North et al. (1982). The first EOF consists in a northeastward–southwestward shift of the continental part of the SACZ from its climatological position (characterized by its mean axis shown as a dashed line in Fig. 4a), while the oceanic part tends to strengthen/weaken. The second EOF shows the opposite behavior, that is, a strengthening of the SACZ over land and a shift over the ocean. The fact that the SACZ does not vary as an integrated structure suggests that the processes governing the variability of the oceanic and continental parts of the SACZ may be different. Figures 1b and 1d hint that the origin of this difference may be in the role of local SST forcing onto the atmosphere. The signal-to-noise optimization analysis discussed below will confirm this finding. However, we caution that this result may depend on the sensitivity of land–atmosphere feedbacks in the model to changes

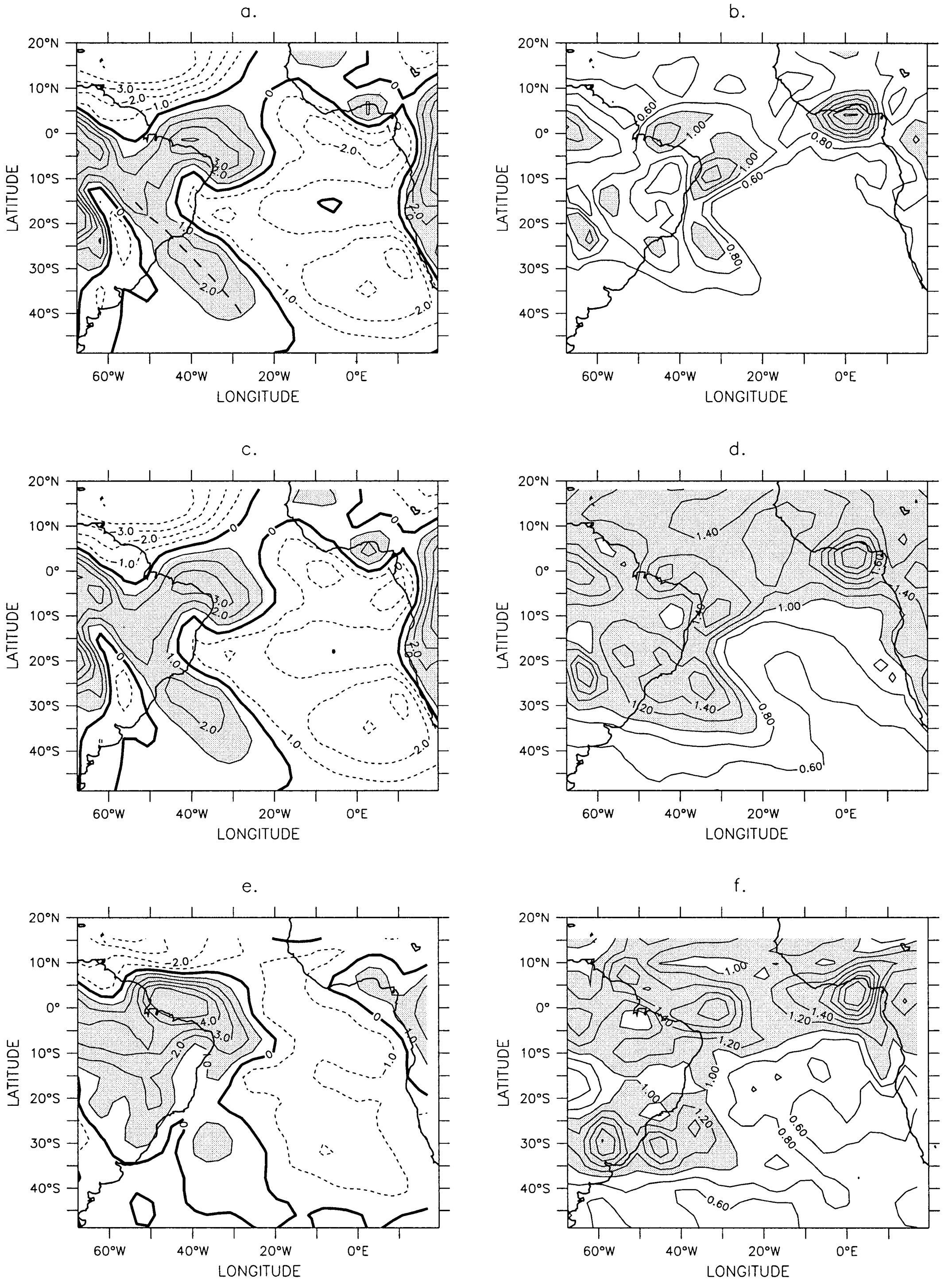

FIG. 2. (left) JFM 200-mb wind divergence climatology and (right) rms variability for period 1958–94 for (a), (b) CCM3 ensemble mean, (c), (d) CCM3 ensemble members, and (e), (f) NCEP reanalysis dataset. In (a) the dashed line marks the mean axis of maximum divergence in the SACZ region. Contour interval is 10^{-6} s^{-1} for climatologies and regions with more than 10^{-6} s^{-1} are shaded. Contour interval is 0.2×10^{-6} s^{-1} for rms maps and regions above 10^{-6} s^{-1} are shaded.

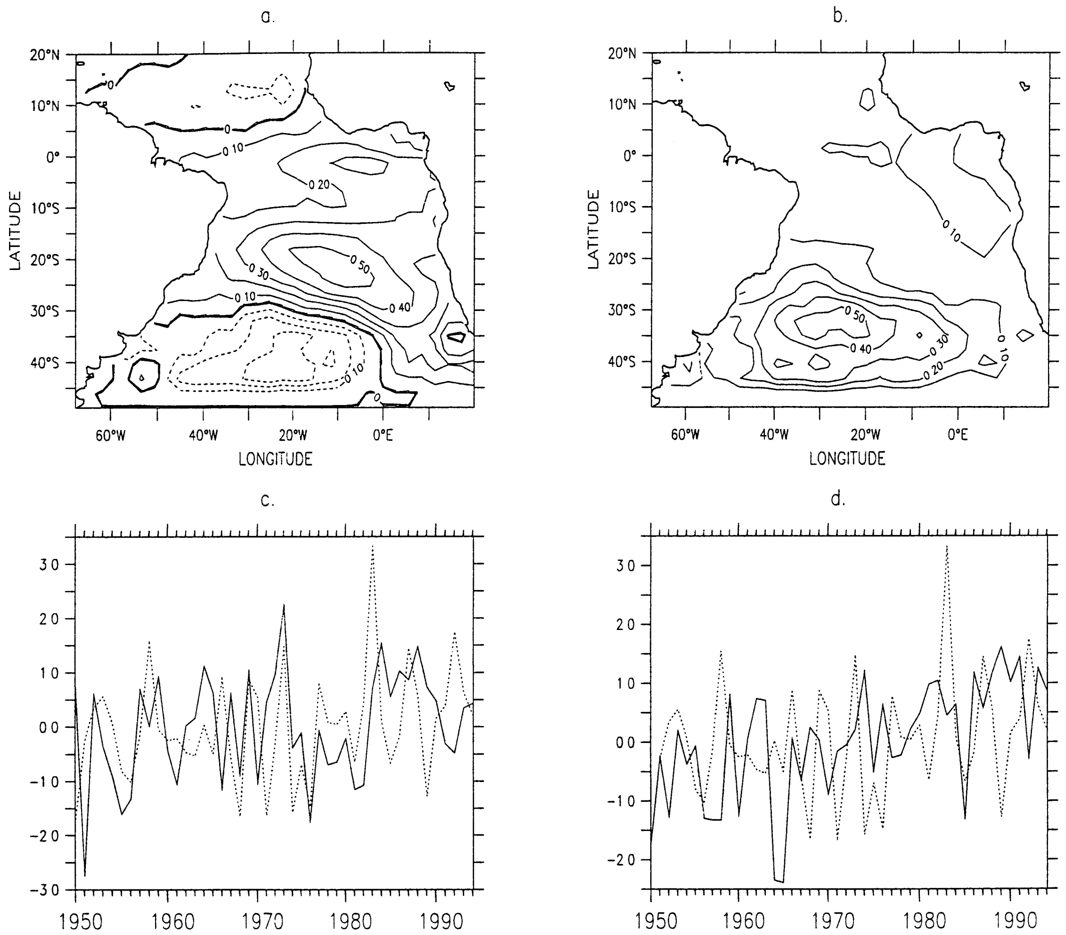

FIG. 3. Leading EOFs of South Atlantic SST variability: (a), (b) the spatial patterns of the first and second EOF, respectively, in units of °C; (c), (d) the associated normalized PCs of first and second EOFs (AT1 and AT2, solid lines) respectively, and the Niño-3 index (dotted line).

in the hydrological cycle. In the CCM3, this sensitivity appears to be rather weak so that changes in SST-forced precipitation does not seem to trigger a strong feedback between the atmosphere and land, and thus the convective activities over the land region of the SACZ are largely independent of changes in SSTs. Other models may behave differently. An intercomparison study with other GCMs is needed to test the robustness of this result.

Figures 4c and 4d show the principal components of leading EOFs associated with each ensemble member. Clearly, there is a large within-ensemble variability, which results from a large internal atmospheric variability. Tables 1 and 2 summarize the correlations between the PCs of each ensemble member and the three indices, that is, Niño-3 index, AT1 (first Atlantic SST mode), and AT2 (second Atlantic SST mode). Only those correlations that are above the 95% significance level according to a Student's *t*-test are shown; values that are below the 95% significance level are indicated by an "*." As expected from the large within-ensemble variability, correlations with the indices vary from one ensemble to another. Interestingly, no PCs of either the first or second EOFs of ensemble members show significant correlation with ENSO. However, some of the PCs do display significant correlation with Atlantic SST anomalies. Since each ensemble member represents a particular realization of the system, there is no a priori reason to judge which ensemble member is more realistic. Therefore, the significant correlation shown by some PCs of ensemble members may occur by chance and would not necessarily mean that there is a real relationship between SACZ precipitation anomalies and the Atlantic SST anomalies.

Next we compare the EOF analysis of the CCM3 ensemble mean with those of individual ensemble members. The first EOF of the ensemble mean is almost identical to Fig. 4a (not shown) and explains 28% of the total variance. The second EOF accounts for 20% of the total variance and is very similar to Fig. 4b (not shown). Table 3 shows the correlation between the ensemble mean PCs and the three indices characterizing ENSO and South Atlantic SST variability. The two leading modes of ensemble mean again show no correlation

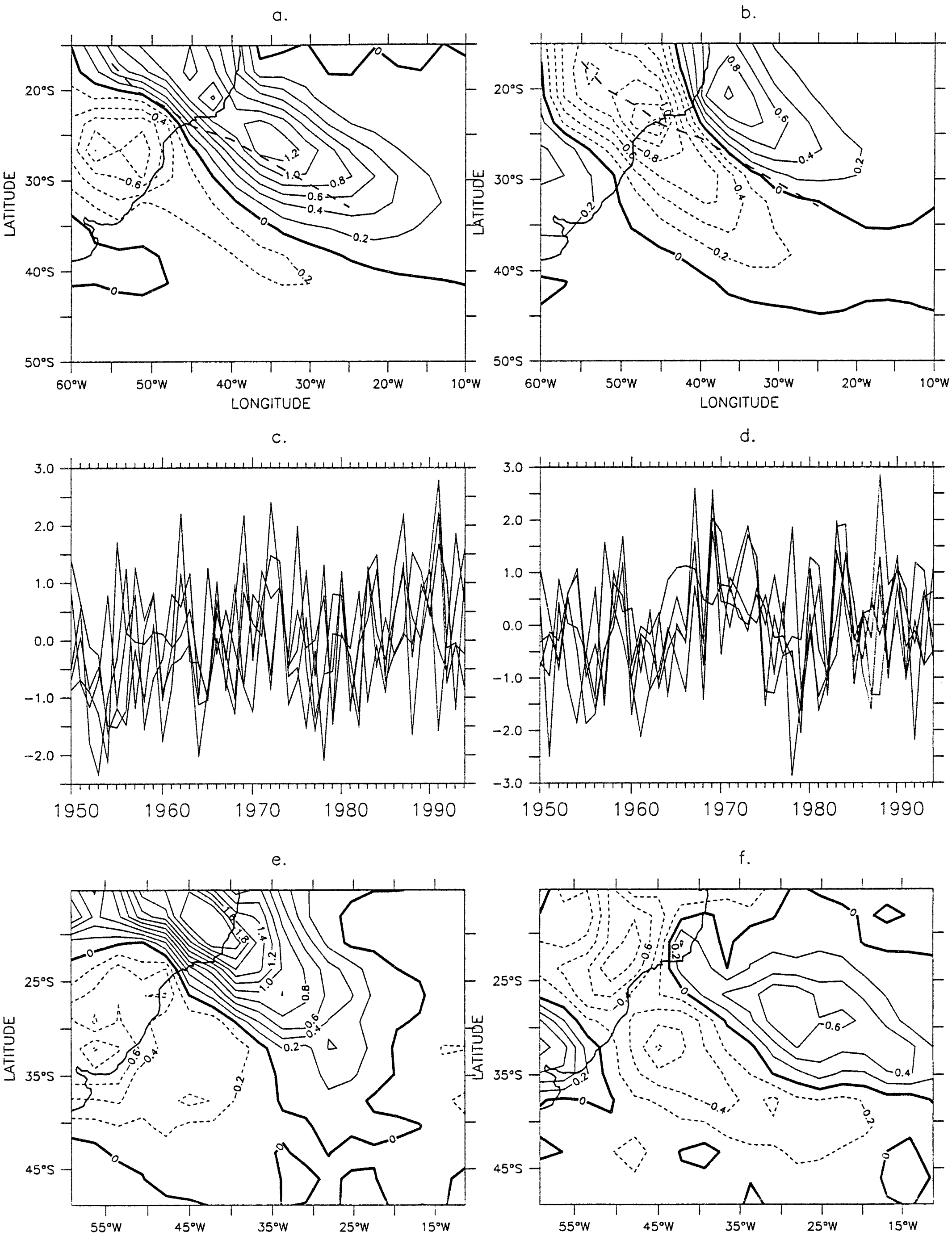

FIG. 4. (top) Leading EOFs of precipitation for CCM3: (a) first EOF, and (b) second EOF. (middle) The PC time series for each CCM3 ensemble member associated to (c) first EOF and (d) second EOF. (bottom) Leading EOFs of Xie–Arkin dataset: (e) first EOF, and (f) second EOF. Units are mm day^{-1} and lines with long dashes in (a) and (b) mark the mean precipitation axis in the SACZ region.

to ENSO SST anomalies. The first EOF of the ensemble mean, on the other hand, shows a high correlation (0.64) with the first Atlantic SST mode, while the second EOF shows a correlation of (−0.52) with the second mode of Atlantic SST variability. Thus, the two leading modes of precipitation in the SACZ region seem to be related to the first two modes of variability of SST in the South Atlantic Ocean, although there are also contributions of the second South Atlantic SST mode to the first precipitation EOF and of the first South Atlantic SST mode to the second precipitation EOF (Table 3).

A similar EOF analysis of the observed precipitation

Table 1. Correlation between the PC time series of the first EOF of precipitation anomalies of each ensemble member and the South Atlantic indices (AT1 and AT2) and Niño-3 index. Here PC- denotes PC time series associated to *i*th ensemble member. The "*" denotes values that are not significant at 95% level.

	PC-0	PC-1	PC-2	PC-3	PC-4
Niño-3	*	*	*	*	*
AT1	0.32	*	0.41	*	*
AT2	−0.34	−0.32	*	*	*

Table 2. The same as in Table 1, except for the second EOF of precipitation anomalies.

	PC-0	PC-1	PC-2	PC-3	PC-4
Niño-3	*	*	*	*	*
AT1	0.37	*	0.34	0.44	0.47
AT2	*	*	*	*	0.33

from the Xie–Arkin dataset results in two EOFs shown in Figs. 4e,f, each of which explains 38% and 12% of the total variance, respectively. Both EOFs exhibit similarity to the corresponding patterns of the CCM3 ensemble members or ensemble mean, particularly for the first EOF (Figs. 4a and 4e). However, the observed EOFs show no significant correlation with ENSO or with South Atlantic SST modes (Table 3).

The above EOF analysis reveals a considerable variability in the temporal behavior of the dominant modes among the ensemble members and ensemble mean. These differences arise because the EOFs are constructed in such a way that they simply maximize the variance explained in a given dataset. Since the total variability consists of both forced and internal variability, the variance explained by these EOFs contains a large fraction of internal variability that varies significantly from one ensemble to another. The EOFs of the ensemble mean give better estimates of forced patterns because the process of averaging filters out some portion of the internal variability. Projections of the individual ensemble members onto EOFs of the ensemble mean show a large spread (not shown). This indicates that even the EOFs of the ensemble mean are not common structures to all ensemble members and thus do not represent the true forced responses of the atmosphere to SST forcing.

In order to separate the forced response of the precipitation field from its internal variability, we performed the signal-to-noise optimization analysis as discussed in section 2 (hereafter called S/N optimals). Results are displayed in Fig. 5. The leading S/N optimal shows a dipole pattern over the South Atlantic Ocean off the coast of South America with almost no loading over land (Fig. 5a). The associated principal component (Fig. 5c, PR1) shows no significant correlation to ENSO, but is highly correlated with the first Atlantic SST mode with a correlation of 0.7, which is significant at the 99% level. The correlation increases to 0.77 when a Parzen filter window of 5 yr is applied. This result lends support to the hypothesis that local SSTs provide a forcing onto the atmosphere. Note that the pattern is similar to the oceanic part of the second regular EOF of precipitation, that is, positive anomalies to the north of the mean SACZ axis and negative anomalies to the south. The fact that there is almost no signal over land is in agreement with the idea that local SST forcing is an important contributor to the variability of precipitation in the oceanic part of the SACZ, but not in the continental part, that is, it is a very localized process. This also implies that precipitation variability is mainly influenced by atmospheric internal variability and that the forced signal is hidden within the total response.

The large-scale circulation structure associated with the dominant forced mode is constructed by regressing SST, surface pressure, surface winds, precipitation, and surface fluxes onto PR1. Regressions are done over the domain from 50°S to 20°N in latitude and from 70°W to 20°E in longitude to better reveal the circulation structure. Figure 6a shows the regression of surface winds and SST onto PR1. The structure of the SST anomalies shows a similar dipole structure as the first South Atlantic SST mode in Fig. 3a with a maximum amplitude of 0.4°C at 20°S. The maximum explained local variance by this mode is about 70% of the total variance near the maximum SST anomaly (darker shading indicates more than 50% of variance explained). Surface wind vectors show anomalous circulation with a maximum wind speed of 1.0 m s^{-1} flowing southward in the ITCZ region and northwestward to the south of the SACZ region. Thus, anomalous winds enhance moisture advection to the northern part of the SACZ and bring drier air to the southeastern part. The anomalous flow converges at (20°S, 30°W) and forms a cyclonic circulation largely in geostrophic balance with the surface pressure anomaly shown in Fig. 6b. At upper levels the circulation anomaly consists of an anticyclonic eddy at the same location (not shown), which is consistent with a Gill-type baroclinic response to a local warm SST anomaly.

The regression of the precipitation is shown in Fig. 6c. It indicates a positive correlation between precipitation and SST anomalies consistent with previous results. This mode accounts for a large portion of the total precipitation variance near the center of maximum precipitation. The location of the maximum precipitation anomaly (0.8 mm day^{-1}) also coincides with the center

Table 3. Correlation between the PC time series of first two leading EOFs of ensemble mean precipitation (first two columns) and of Xie–Arkin dataset (last two columns) and the South Atlantic indices (AT1 and AT2) and Niño-3 index. The "*" denotes values that are not significant at 95% level.

	PC1em	PC2em	PC1xa	PC2xa
Niño-3	*	*	*	*
AT1	0.64	0.34	*	*
AT2	0.35	−0.52	*	*

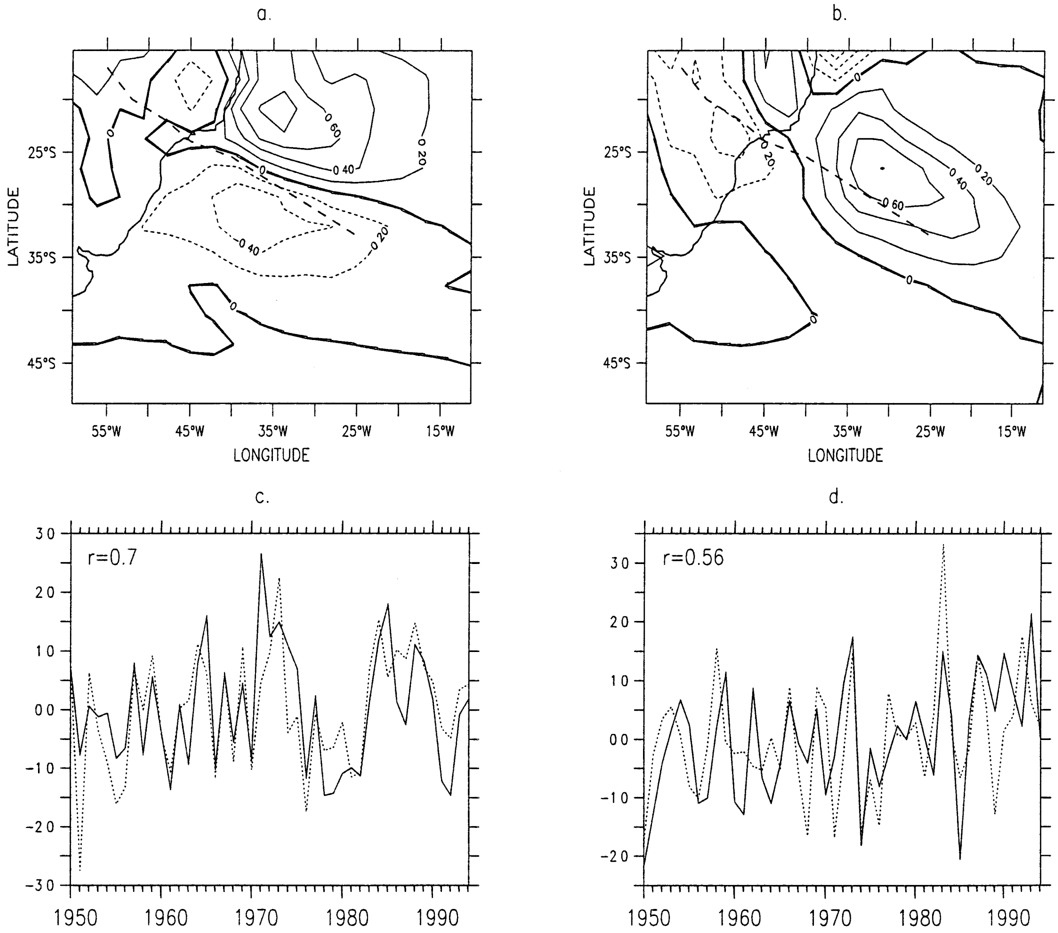

FIG. 5. The S/N optimal patterns for precipitation in mm day^{-1}: (a) the first dominant forced response and (b) second dominant forced response. (c) The PC time series of the first S/N optimal (PR1, solid line) and of the leading South Atlantic mode of SST variability (AT1, dotted line). (d) PC time series of the second S/N optimal (PR2, solid line) and Niño-3 index (dotted line). In (a) and (b), the dashed lines marks the mean precipitation axis in the SACZ region.

of convergence and of largest negative anomaly in surface pressure. Note that the center of maximum precipitation is displaced from the center of maximum SST anomalies toward the land. Figure 6d shows the regression of the downward heat fluxes onto PR1. As can be seen, in subtropics the flux anomalies have opposite signs to the SST anomalies, indicating a negative feedback in which the atmosphere damps the SST anomalies. On the contrary, in the deep Tropics the SST and heat flux anomalies have the same sign, suggesting the existence of a positive feedback (see Chang et al. 2000). These results clearly support the hypothesis of local SST forcing the atmosphere through modifications of the boundary layer stability properties by enhanced atmospheric latent heat fluxes.

Heat flux anomalies in the deep Tropics resemble the pattern associated to the Atlantic "dipole" (see Chang et al. 2000). Also, Figs. 6a and 6c suggest that when the SACZ moves northward, the ITCZ moves southward as the warm anomaly of the dipole develops in the south tropical Atlantic. Therefore, the first EOF of SST anomalies in the South Atlantic Ocean seems to be related to the tropical Atlantic dipole. A further exploration of the relationship between the SACZ and ITCZ and its relationship to the Atlantic dipole is, however, beyond the scope of this study.

The second S/N optimal of precipitation shows mainly a strengthening (weakening) of the northern oceanic portion of the SACZ and a shift over the land (Fig. 5b), capturing some features of the first regular EOF. The associated PC (PR2) is correlated to ENSO ($r = 0.56$; Fig. 5d), and also to both the first and second Atlantic SST modes of variability with $r = 0.36$ and $r = 0.53$, respectively. Therefore, this precipitation pattern seems to result from both local and remote SST forcing. The structure of this mode is shown in Fig. 7. Regressing South Atlantic SST onto PR2 gives rise to a pattern that shows two local maximums at (25°S, 10°W) and at (25°S, 35°W). Figure 7b shows that the anomalous circulation is mostly in geostrophic balance with the pressure anomaly. The regression of precipitation (Fig. 7c) shows that the maximum explained variance is over the

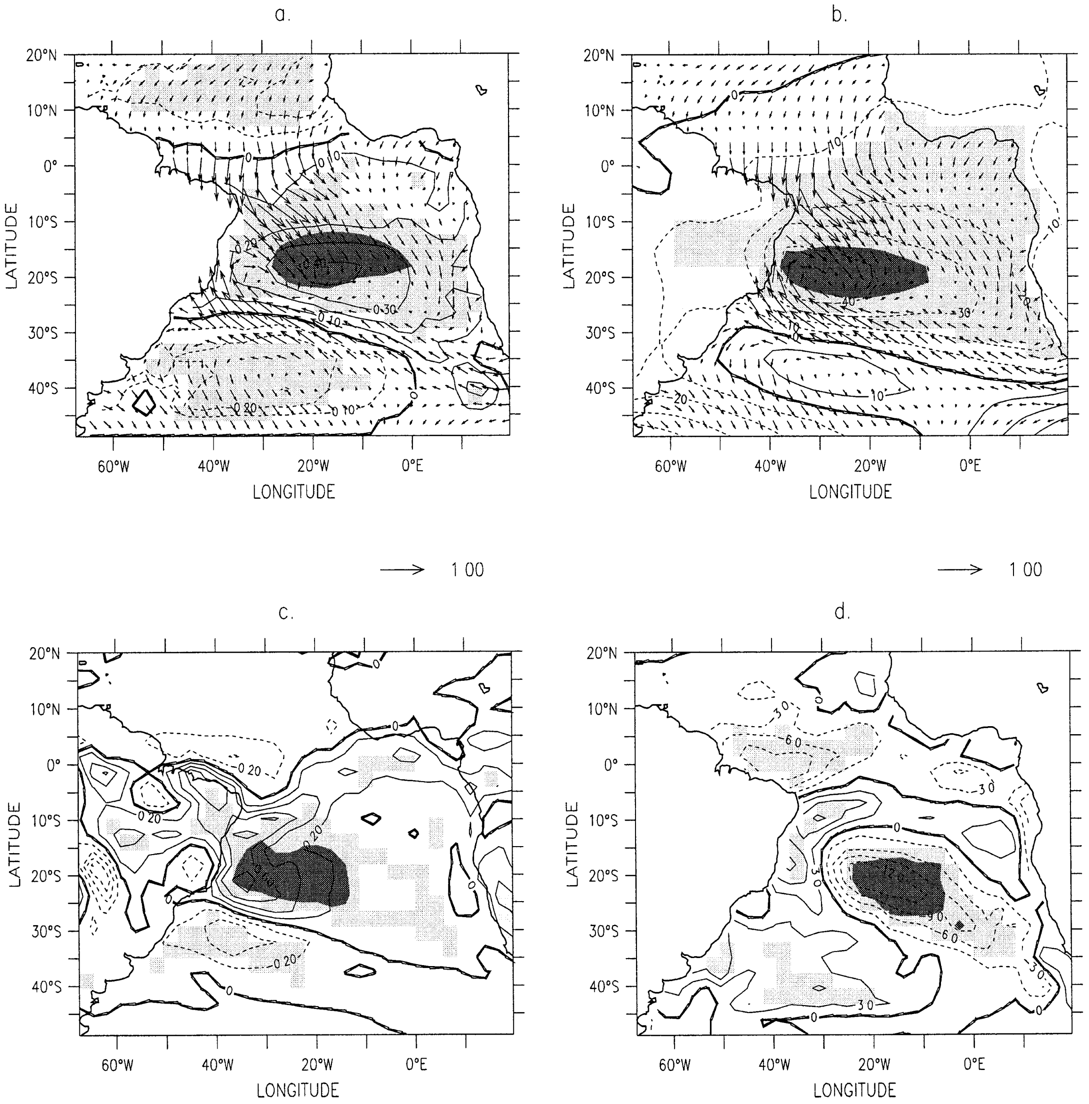

FIG. 6. Three-dimensional structure of the leading S/N optimal constructed by regressing (a) SST (°C) and surface winds anomalies (m s^{-1}), (b) pressure (Pa) and surface wind anomalies, (c) precipitation (mm day^{-1}), and (d) downward surface heat fluxes (W m^{-2}), onto PR1. Arrows located beneath (a) and (b) indicate wind anomalies of 1 m s^{-1}. Shaded areas in all panels indicate significance at the 95% level; darker shading indicates regions where explained variance is ≥50%. In (a), shaded areas are for SST anomalies and in (b), shaded areas are for pressure anomalies.

ocean. Significant precipitation anomalies also exist over the land, suggesting a northward shift of the SACZ. It is interesting to note that the anomalies in the SACZ and ITCZ regions have opposite signs. Finally, the flux anomalies appear as a dipole at both sides of the SACZ main position (Fig. 7d). The northern component has the same sign as the SST, suggesting a positive feedback, whereas the southern component has the opposite sign as the SST, suggesting a negative feedback.

In order to see if the precipitation patterns found by the signal-to-noise optimization procedure are common to all the ensemble members we project each ensemble member onto the filter patterns associated to the S/N optimals (dotted lines in Fig. 8). The spread of individual members around the ensemble mean is much reduced compared to the case of conventional EOF analysis, indicating that the patterns found are common to all ensemble members. This shows that the algorithm has been successful in extracting the true forced response and filtering out the internal variability. Projections of the Xie–Arkin dataset onto the filter patterns show time series that appear to follow nicely to the variations of model forced responses, especially after 1982. This implies that the model captures a forced response to SST forcing that seems to exist not only in the ensemble simulations but also in the real world, although certain caution must be taken in interpreting the observations because of the shortness of record length.

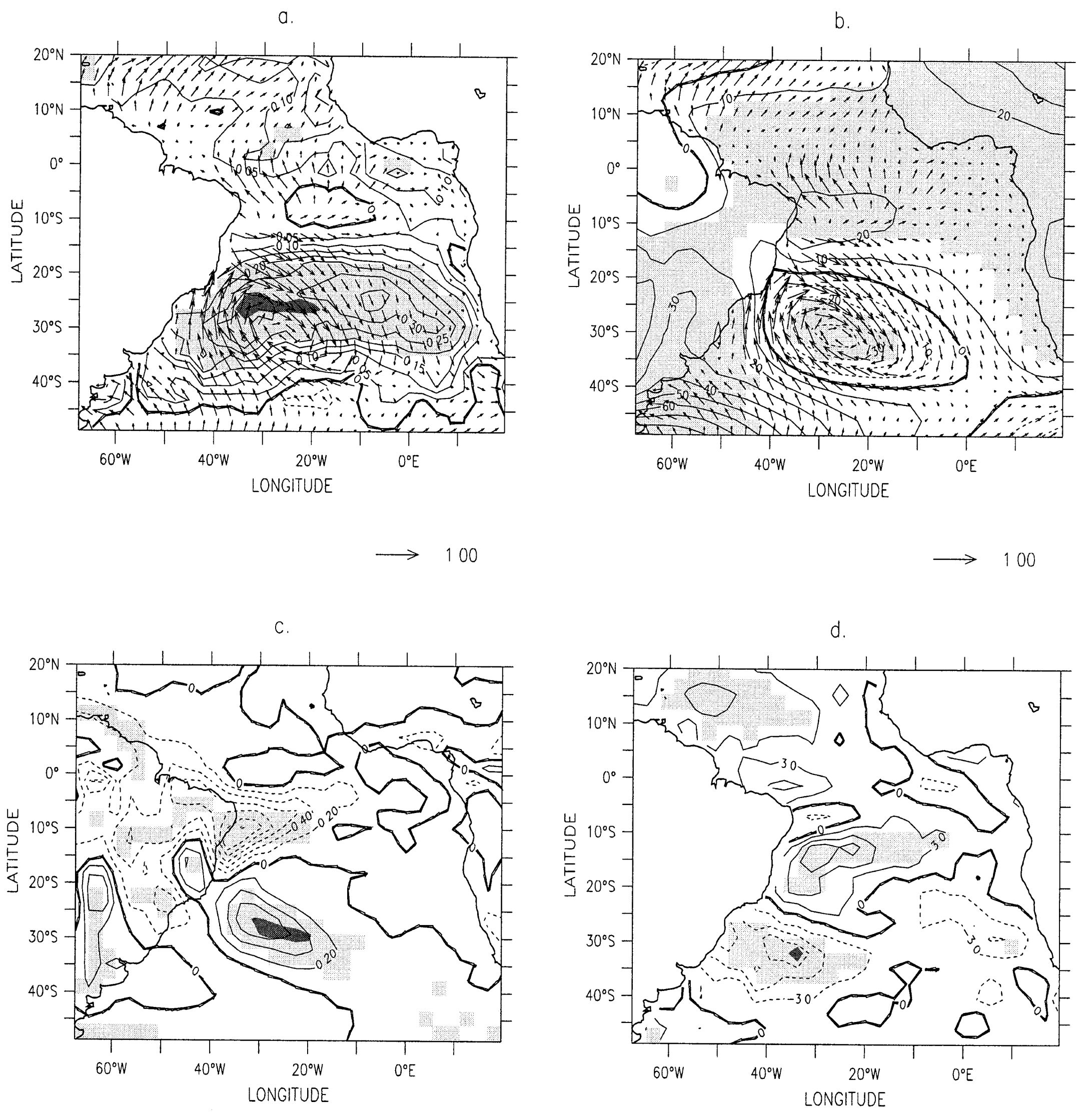

FIG. 7. The same as Fig. 6, except for the second S/N optimal of precipitation.

b. Variability of upper-level wind divergence

Precipitation variability results from changing conditions over the whole depth of the atmosphere, that is, it depends on lower- and upper-level conditions and consequently reflects an integrated effect. In this section we use the upper-level wind divergence mostly as a measure of upper-level variability. Precipitation and upper-level divergence are not always correlated because while strong precipitation is often associated with upper-level divergence, the converse is not always true. As we will find below local responses are seen mainly in lower-level fields, while remote influences are felt in upper levels. Thus, the use of upper-level wind divergence, which has been often used as a proxy for the location and intensity of the SACZ (Kodama 1992, 1993), is adequate to study remotely forced perturbations in the SACZ.

Similar analyses to the precipitation were performed to the wind divergence. Figures 9a and 9b show the patterns of leading EOFs of the covariance matrix formed by concatenating the ensemble members. The first EOF explains 29% of total variance and the second EOF explains 18% of total variance. Again, the temporal behavior of the patterns differs considerably among ensemble members, indicative of a large atmospheric internal variability (Figs. 9c and 9d). In contrast with the precipitation case, the divergence EOF patterns show a consistent behavior over the whole SACZ region. The first EOF presents a northeastward–southwestward displacement of the whole SACZ from its climatological position (marked as dashed line in Fig. 9a). Unlike precipitation, however, none of these leading PCs except two show significant correlation to the Atlantic SST anomalies, and two of them show significant correla-

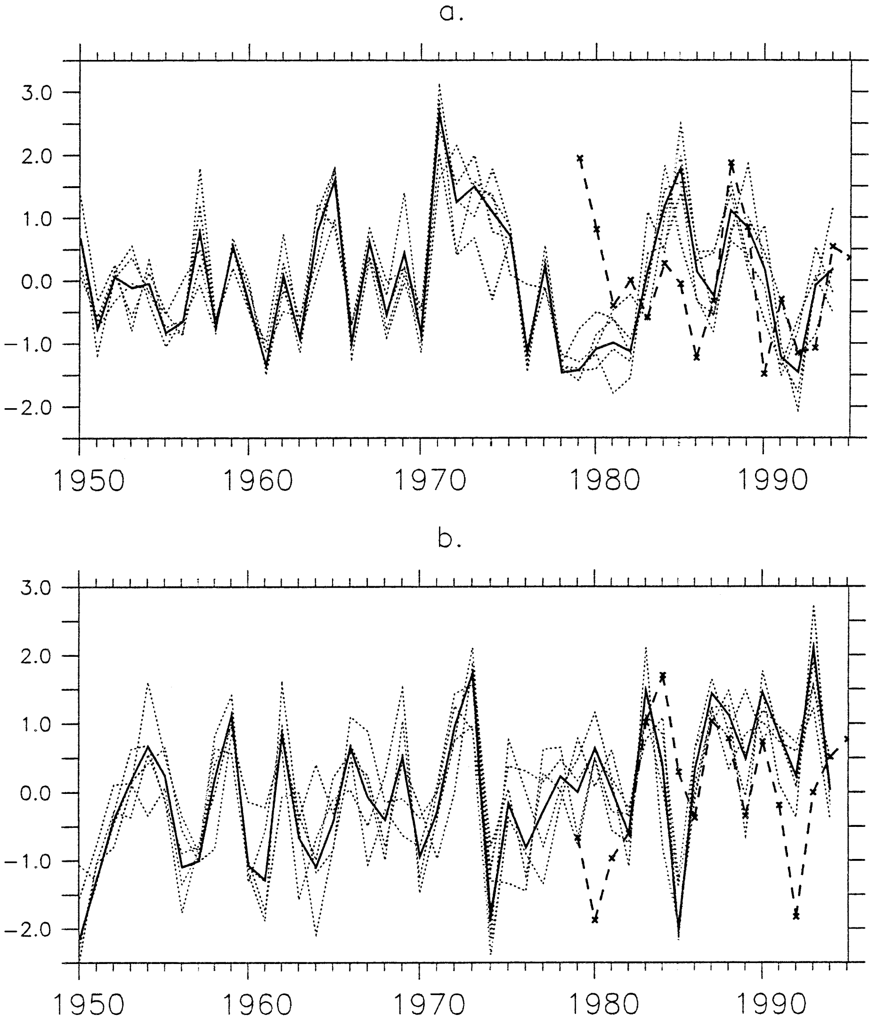

Fig. 8. PC time series of the forced precipitation responses (solid lines) superimposed on the projections of CCM3 ensemble members (dotted lines) and of the Xie–Arkin dataset (dashed line) onto the optimal filter patterns: (a) first S/N optimal and (b) second S/N optimal.

tions to ENSO (Table 4). The second EOF is statistically different from the first and third EOFs according to the North et al.'s rule. It shows a strengthening (weakening) of the whole SACZ, and the PCs do not show significant correlation with any SST index.

The first two leading modes of the CCM3 ensemble mean are similar to the first and second EOF modes shown in Figs. 9a and 9b (not shown) and explain 37% and 17% of total variance, respectively. The first EOF is well correlated to ENSO, but only weakly correlated to the South Atlantic SST modes (Table 5). Therefore, this mode of variability seems to be mostly remotely forced and only weakly influenced by local SST. The second EOF of ensemble mean does not show significant correlation with any SST indices according to Table 5.

The two leading EOFs calculated for the NCEP reanalysis dataset explain 25% and 20% of total variance and are shown in Figs. 9e and 9f. The structure of the second NCEP EOF show some similarities to the first ensemble members EOFs. However, the NCEP EOFs show no correlation to ENSO and no significant correlation to Atlantic SST modes of variability (Table 5).

Projections of individual ensemble members onto the ensemble mean EOFs show large spreading around the ensemble mean (not shown), suggesting that the upper-level response contains substantial internal variability. This implies that the first ensemble mean EOF does not reflect the true forced signal, despite its significant correlation to the local SST indices shown in Table 5.

The leading SN optimal shows a forced response in the form of a northeast–southwest shift of the SACZ from its climatological position (Fig. 10a). The signal is particularly clear for the region of the SACZ over land. Over the ocean the pattern represents more a strengthening (weakening) of the northern part of the SACZ than a shift from its mean position. The correlation between the associated PC (DI1) and Niño-3 index is 0.70 (Fig. 10c), implying that during warm ENSO

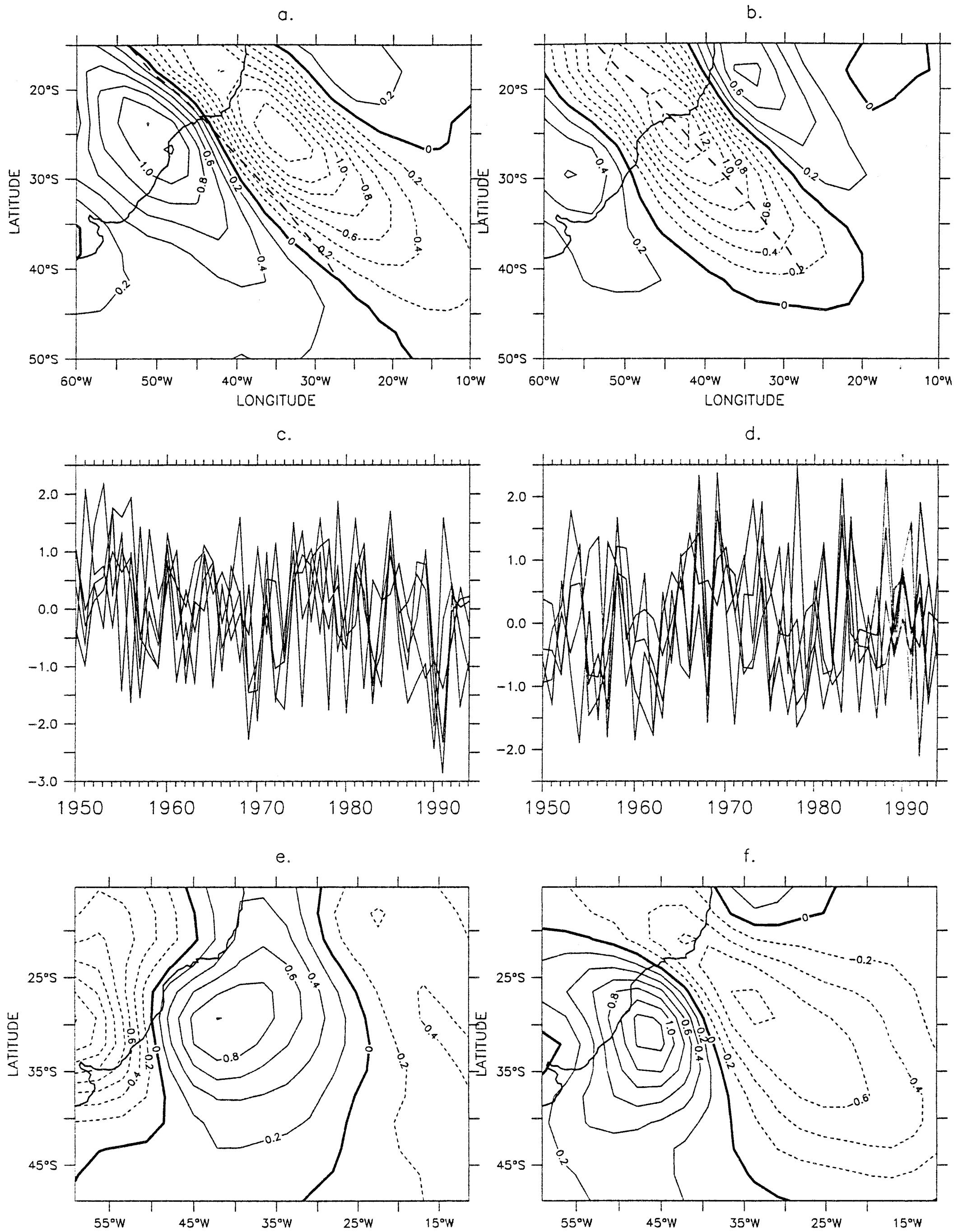

FIG. 9. (top) Leading EOFs of 200-mb wind divergence for CCM3: (a) first EOF, and (b) second EOF. (middle) The PC time series for each CCM3 ensemble member associated with (c) first EOF and (d) second EOF. (bottom) Leading EOFs of NCEP dataset: (e) first EOF and (f) second EOF. Units are 10^{-6} s^{-1} and dashed lines (a) and (b) mark the mean axis of maximum divergence in the SACZ region.

events the upper part of the SACZ tends to displace northeastward over the land and strengthen over the ocean. The associated sea level pressure anomaly (Fig. 10b) indicates a northward shift of the South Atlantic subtropical high from its climatological position in agreement with early studies of ENSO influence in this region (e.g., Peixoto and Oort 1992). The anomalous surface winds show convergence to the north of the SACZ mean position that is consistent with the northeastward shift of the South Atlantic subtropical high. The regression map of precipitation onto DI1 (Fig. 10d) indicates a weakening of the ITCZ, accompanied by the

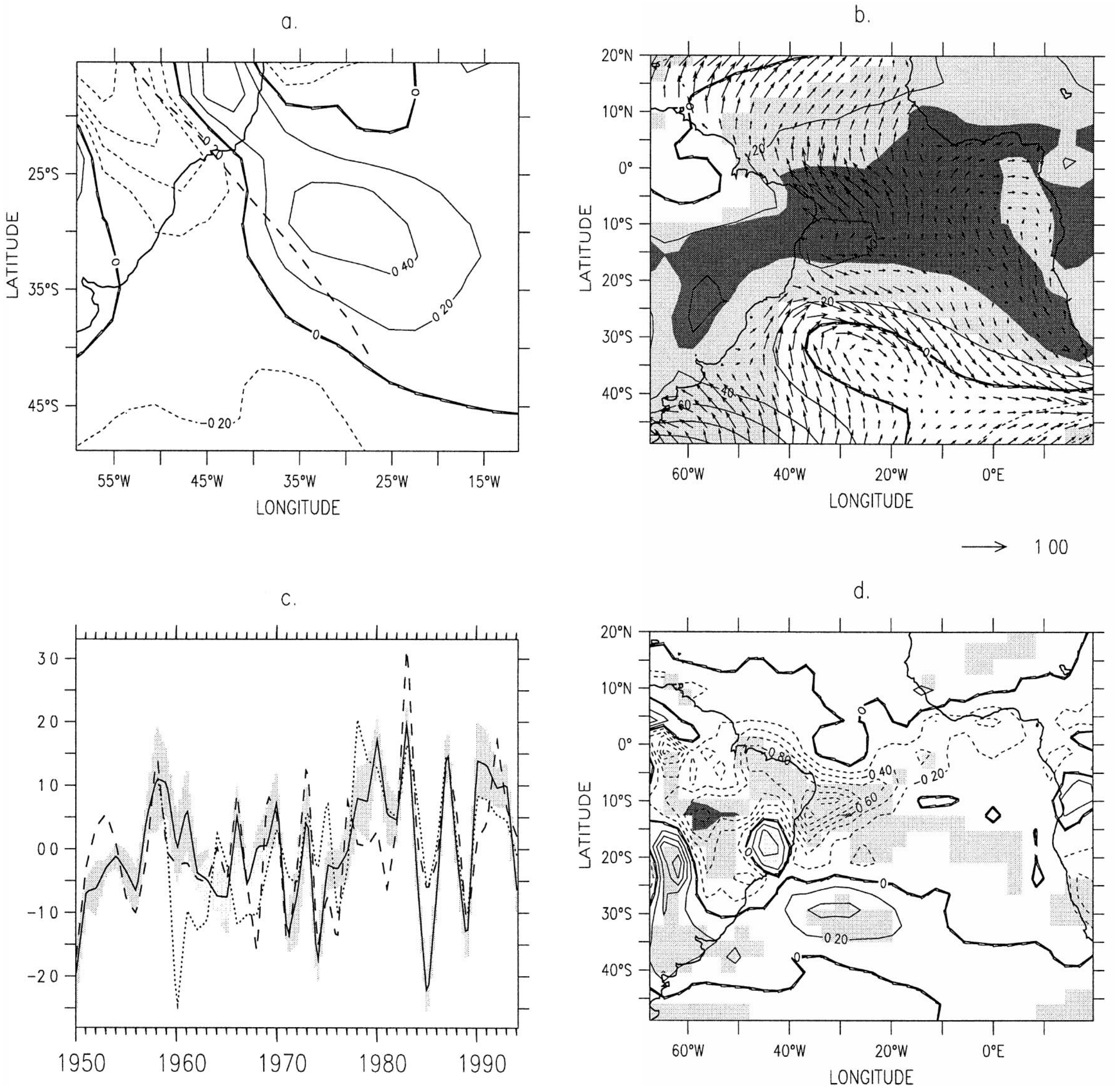

Fig. 10. (a) Leading S/N optimal pattern of 200-mb wind divergence. The dashed line marks the mean axis of maximum divergence in the SACZ region. (b) The associated surface winds and surface pressure anomalies (contour interval is 20 hPa). Arrow indicates wind anomalies of 1 m s^{-1}, and shaded areas are pressure anomalies significant to 95% level. (c) The associated time series (DI1, solid line) and Niño-3 index (dashed line). Superimposed are the projections of NCEP reanalysis dataset onto the optimal filter pattern (dotted line). Shading shows standard deviation of projections of ensemble members onto optimal filter pattern about DI1. (d) The associated rainfall anomalies, and shading indicates areas significant to 95% level. Darker shading in (b) and (d) indicates regions where explained variance is $\geq$50%.

change of precipitation in the SACZ region. The negative rainfall anomaly in tropical regions indicates a weakening and possible northward shift of the ITCZ during warm ENSO events. The southeasterly wind anomalies in the western equatorial Atlantic supports this notion. No significant correlation between DI1 and the Atlantic SST modes of variability is found. However, DI1 shows a correlation of 0.61 with the second S/N optimal of precipitation (PR2) suggesting that the second dominant pattern of precipitation is linked to the variability in the upper atmosphere. The similarity between the anomalous rainfall and surface circulation fields in Figs. 7b and 7c with 10b and 10d strengthens this finding. We will show below that the close relationship between the two modes can be attributed to the fact that both these modes are induced by remote ENSO influence.

The reduced spread of the projections of ensemble members onto the associated optimal filter of the leading S/N optimal pattern of divergence confirms that the leading forced mode is in fact a structure common to all ensemble members. The projection of the NCEP reanalysis dataset follows very closely to the ensemble mean projection, implying that the forced CCM3 re-

TABLE 4. Correlation between the first EOF of 200-mb wind divergence anomalies of each ensemble member and the South Atlantic indices (AT1 and AT2) and Niño-3 index. The PC- denotes PC time series associated with the *i*th ensemble member. The "*" denotes values that are not significant at 95% level.

	PC-0	PC-1	PC-2	PC-3	PC-4
Niño-3	0.42	*	0.38	*	*
AT1	*	*	*	−0.34	*
AT2	*	*	*	*	−0.35

TABLE 5. Correlation of first two leading EOFs of ensemble mean 200-mb wind divergence (first two columns) and of NCEP dataset (third and fourth columns) and the South Atlantic indices (AT1 and AT2) and Niño-3 index. The "*" denotes values that are not significant at 95% level.

	PC1em	PC2em	PC1ncep	PC2ncep
Niño-3	0.52	*	*	*
AT1	0.37	*	*	*
AT2	0.36	*	*	*

sponse of the upper-level wind divergence seems to be also present in the real world (Fig. 10c). The fact that the leading S/N optimal is more significantly correlated to ENSO than to the South Atlantic SSTs suggests that the upper-level divergence seems to be principally forced by the SST anomalies in the tropical Pacific Ocean, but not influenced so much by the local Atlantic SST anomalies. This result contrasts sharply to the finding of the precipitation field analysis, which shows a dominant response to local Atlantic SST anomalies. Because of the strong local SST influence on the oceanic part of the SACZ, the variability of the precipitation over the ocean appears to be disconnected from its continental part. On the other hand, the upper-level winds are not affected by local SST and therefore the divergence in the SACZ region varies as one structure (Figs. 4a,b and 9a,b).

In addition to the above analyses, we have also made composite maps associated with the warm ENSO events by averaging all the anomalies where positive values of DI1 exceed one standard deviation. These maps reveal similar spatial patterns as shown in Figs. 10b and 10d. However, the composite anomalies are stronger and more sharply defined than those in the regression analyses. In contrast, the composite anomalies of cold ENSO events are generally weaker than the regressed anomalies, particularly over the oceanic portion of the SACZ (not shown). This may imply a nonlinear nature of the SACZ response to ENSO influence. Further studies are needed to understand the difference between SACZ responses to warm and cold ENSO events.

To get a global view on how ENSO forcing propagates into the Atlantic, Fig. 11 shows the regression of upper-level wind anomalies onto DI1 in the whole tropical–subtropical band. It clearly shows the observed anticyclone straddling the equator forced by convective anomalies associated with warm ENSO events. The figure also reveals a propagating wave pattern emanating from the tropical Pacific. This supports the notion that a remote influence from the tropical Pacific Ocean occurs in the form of a wave train (cf. Hoskins and Karoly 1981). Associated with this pattern is also a strengthening/weakening of the subtropical westerly jet between 20° and 30°S. Close to the coast of southern Brazil and Uruguay the flow tends to be organized as an upper-level cyclonic eddy. Comparing with the low-level winds in the same region (Fig. 10b) we conclude that the eddy has a barotropic structure because anomalies have the same sign at upper and lower levels. This is in contrast with the baroclinic response of the atmosphere to local SST forcing seen in section 4a.

In order to find the coherent behavior of upper-level wind divergence and precipitation, we apply the same analysis to both fields simultaneously. It was found that the leading joint mode consists of the first S/N optimal for divergence and of the second S/N optimal for precipitation (not shown). The joint mode also shows a correlation of 0.7 with Niño-3 index. This result, to-

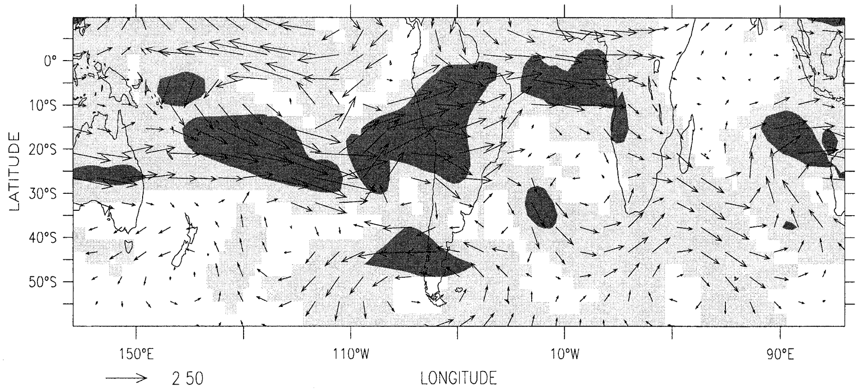

FIG. 11. Regression of 200-mb wind anomalies onto DI1. Units are in m s^{-1}. Shading denotes that at least one wind component is significant to the 95% level; darker shading indicates regions where explained variance is ≥50%.

gether with previous findings about the similarities between the first S/N optimal of divergence and the second S/N optimal of precipitation, further suggest that these two patterns represent a single coherent structure of remotely forced SACZ variability by ENSO.

The picture emerging from above analyses is as follows. The precipitation anomalies in the SACZ region have two sources of influence: 1) a local influence due to Atlantic SST variability at interannual-decadal timescales that may be the result of modifications of the boundary layer stability properties by changes in the latent heat fluxes, and 2) a remote influence due to Pacific SST variability (at interannual timescales), which modifies the large-scale upper-level circulation and produces changes in precipitation. The strong tie to surface conditions can be understood by the fact that the SACZ, as the ITCZ, is a convective system that is dependent on surface SST and heat fluxes. Remote forcing from the Pacific leads to a barotropic cyclonic eddy off the east coast of South America. Although associated wind anomalies are weaker at the surface than at upper levels, they propitiate precipitation anomalies by advecting dry air to the southern part of the SACZ, and bringing moist air from the northwest to the northern part of the SACZ.

c. Removing remote ENSO forcing

To further separate the ENSO forcing from local processes while keeping intact the atmospheric response to local Atlantic SST, we regress the precipitation and 200-mb wind divergence fields of each ensemble member onto Niño-3 index and then remove this part of the signal from the total fields to form a residual field. We then apply the signal-to-noise optimization analysis to the residual precipitation and upper-level wind divergence. We found that the first and second optimals of precipitation on the residual field are nearly identical to those without removing ENSO. Moreover, upon removing the ENSO influence the correlation between the time series associated with the first optimal and the first Atlantic SST mode increases to 0.77, and the correlation between the time series associated with the second optimal and the second Atlantic SST mode increases to 0.76. Therefore, this study suggests that the dominant SST-forced precipitation signal in the SACZ comes from neither the direct nor indirect ENSO influence, instead it comes from the SST anomalies locally generated in the South Atlantic.

Similar analysis to the upper-level divergence field did not yield a clean result. This may be due to the fact that ENSO dominates the dynamics of upper levels, so that its removal will leave patterns that contain a large portion of internal atmospheric variability and only a small portion of locally forced signal. This makes the signal-to-noise optimization procedure difficult to apply.

5. Summary and discussion

a. Summary

In this paper we focus on the variability of the SACZ at interannual and decadal timescales during austral summer (season JFM). An attempt is made to separate the forced variability from the internal variability. This is accomplished by applying a signal-to-noise optimization analysis to an ensemble of multidecadal CCM3 integrations forced with observed SST. Conventional EOF analysis was also performed for two variables characterizing the SACZ, that is, precipitation and 200-mb wind divergence. In order to relate the SACZ variability to the SST anomalies, we correlate the PC time series of the EOFs with three indices characterizing SST variability of the eastern equatorial Pacific Ocean (Niño-3) and of the Atlantic Ocean (first two leading mode normalized PCs). Our major findings are the following:

- A significant portion of the subtropical atmosphere is governed by atmospheric internal dynamics. In the CCM3, approximately 59% of the total variance in the SACZ region can be attributed to the internal atmospheric variability. For comparison, only about 20% of total precipitation variance is accounted for by internal dynamics in the ITCZ region. This suggests that the SACZ region may have much less potential predictability than the ITCZ region.
- The modeled precipitation field shows a forced response to local anomalous SST in the Atlantic Ocean on decadal timescales (particularly after the 1970s). It is well correlated with the first EOF of austral summertime South Atlantic SST that consists of a dipolelike SST anomaly centered at around 25°S. This pattern of SST creates a dipolelike structure in precipitation close to the coast of South America shifting the SACZ to the northeast together with a clockwise anomalous circulation of surface winds that is in geostrophic balance with the anomalous pressure. The response is localized within the South Atlantic Ocean with almost no signal over land, although there seems to be a simultaneous southward displacement of the ITCZ.
- Upper-level wind divergence shows a forced signal closely related to ENSO and is largely independent of Atlantic SST variability. This remotely forced response, which seems to occur also in the real world, has interannual timescales and produces a northeastward shift and strengthening of the SACZ during warm ENSO events. These results are in agreement with the outgoing longwave radiation (OLR) anomaly in an observational work by Aceituno (1988). Model results show that the SACZ tend to shift over the land and that the northern oceanic part of the SACZ strengthens during warm events.

b. Discussion

The above results suggest two possible interrelated mechanisms through which ENSO can exert its influence on the SACZ. First, our results show that warm ENSO events weaken the intensity of the Atlantic ITCZ in the SH summer season (Fig. 10d) in agreement with Aceituno (1988) and Saravanan and Chang (2000). In the SH summer season the Hadley cell is already weak compared with the SH winter cell. Therefore, a decrease in the ITCZ intensity during ENSO will make it even weaker. Also, the generation of a cyclonic anomaly off the coast of southern Brazil and Uruguay weakens the subtropical high locally. Consequently, the South Atlantic subtropical high becomes weaker and the poleward surface flow in its western flank diminishes. This is consistent with a northward shift of the subtropical high during warm ENSO events (Peixoto and Oort 1992), as shown in Fig. 10b. At the same time, the northern portion of the upper-level subtropical westerly jet appears to be strengthened in the Pacific sector and South American continent between 20° and 30°S (Fig. 11). According to Kodama (1993), the location of the SACZ is given by the convergence region between the subtropical jet in the subtropics and the low-level poleward flow. In agreement with Kodama (1993) we found that the conditions of a weaker surface poleward flow and an anomalously strong westerly jet shifts the convergence zone to the northeast of its climatological position. This causes a decrease in precipitation in the climatological position of the SACZ that is further enhanced by the advection of dry air from the southeastward caused by the anomalous eddy. Cook (2000) reported a similar northeastward shift of the South Indian convergence zone during warm ENSO events.

On the other hand, the changes in the basic state associated with ENSO (Fig. 11) and the shift of the mean position of the SACZ are consistent with the work of Matthews and Kiladis (1999). They found that during the so called ''strong (NH) winters'' (an index with correlation of 0.9 to Niño-3.4 index) Rossby wave–like transients are found to propagate preferentially along the strengthened subtropical jet that acts as a waveguide. This finding is in line with the barotropic Rossby wave theory. Kiladis and Weickmann (1992) found that convection in the SACZ is modulated by upper-level wave activity in the westerlies. Our analysis suggests that this mechanism may be operating on interannual timescales in the SACZ region. During warm ENSO events, we have seen evidences for the strengthening of the subtropical jet (Fig. 11b). Accompanying the strengthened westerly, we have observed wavelike disturbances propagating along the subtropical jet deep into the south tropical Atlantic, possibly triggering convection and shifting the mean position of the SACZ northeastward. This result seems to be consistent with the mechanism suggested by Matthews and Kiladis (1999); in their Fig. 3c anomalous negative OLR is seen to the north of the main position of the SACZ in a composite map of strong (NH) winters minus ''weak winters.'' The result is also in agreement with the work of Figueroa et al. (1995) who found that inclusion of climatological flow can change the position of the SACZ.

Furthermore, Kalnay et al. (1986) reported observational evidence of a stationary Rossby wave during January 1979 situated at about (30°S, 50°W) associated to an intensification of the SACZ. They suggested that tropical heating could generate the waves and that a Walker-type circulation associated with the SPCZ helps in their maintenance, pointing to the importance of ENSO events in modulating the convective activity in the SACZ and SPCZ. Actually, the strengthening of the SACZ in their Figs. 5a and 6a, seems to be accompanied by a northeastward displacement of the convergence zone from its mean position. Our findings seem to support their result that the upper-level circulation in the SACZ region on interannual timescales is mainly remotely influenced by ENSO, and that warm ENSO events increase convective activity in the SACZ region.

Robertson and Mechoso (2000) performed EOF analysis to NCEP reanalysis data in the South American region. Their first EOF shows a strong upper-level cyclonic eddy, associated with the intensification of the SACZ. The center of the eddy was situated at (30°S, 40°W) and has a zonal wavenumber 6, slightly larger than the scale reported by Kalnay et al. (1986). A vorticity budget analysis showed that the eddy has the characteristics of a locally forced stationary Rossby wave, and shows no correlation to ENSO. They further argue that this circulation anomaly produces a surface heat flux anomaly that generates an SST anomaly in the South Atlantic. Although they suggest that this SST anomaly may increase the persistence of the SACZ anomalies through reduced thermal damping, their results hint that changes in the SACZ are largely internally driven. Robertson and Mechoso (2000) also reported a second EOF that is correlated to ENSO that shows similar upper-level structure as our first S/N optimal of the divergence field, but does not seem to be connected to the SACZ variability. We can assimilate their results with ours as follows. Our results are based on a signal-to-noise optimization procedure applied to a 5-member ensemble run to extract the dominant-forced atmospheric response to local SST forcing. Accordingly, our results should give a better estimate of the forced response in the SACZ region, which is likely to differ from the leading pattern of internal variability. To check this we calculated the first EOF of the 200-mb wind field of each ensemble member and found an eddylike pattern with similar characteristics as the ''eddy'' structure found in the first EOF of Robertson and Mechoso (2000). We then calculated the correlations of the associated PCs with Niño-3 index and found that only 2 of the 5 ensemble members showed significant correlation. This suggests that an eddylike circulation may be a preferred mode of internal atmospheric variability at upper levels in the SACZ region. This, however, does not mean that SST anomalies have no impact on the variability of the SACZ. The S/N optimization procedure filters the internal variability and gives (ideally) only forced patterns. Accordingly, our first divergence S/N optimal resembles their second EOF, and not their first one. Interestingly, these two patterns are very similar in the deep tropical area, but differ in the extratropics where internal variability is larger, suggesting that the second EOF of Robertson and Mechoso (2000) includes both forced and internal variability. This may be the cause why they suggest that their second EOF is not connected to the SACZ variability, while we showed above that our first divergence S/N optimal is indeed associated with precipitation anomalies in the SACZ region.

In terms of mechanisms for local SST influence, we have presented a modeling evidence that the SST anomaly in the South Atlantic can have certain influence on the SACZ variability, possibly through modifying stability properties of the atmospheric boundary layer and moisture supply needed for the development of deep convection. This local oceanic effect appears to operate on interannual-decadal timescales, and has been found quite localized, with the strongest influence region close to the coast of southern Brazil where a warm SST tongue exists during the SH summer (Fig. 1a). It is possible that the thermal inertia of the ocean may act as a stabilization mechanism of atmospheric anomalies leading to an increase of their persistence (Bladé 1997). This implies that the precipitation associated with the oceanic part of the SACZ region may have some predictability due to the slow SST evolution, but its land component may be mostly unpredictable. This latter result may be highly model dependent and sensitive to a different parameterization of land surface processes. A further intercomparison study using different atmospheric GCMs with distinct land surface models is needed in order to address the importance of the land surface moisture state on the precipitation predictability over land.

Finally, we wish to point out that the results reported here were based on CCM3 simulations forced with global SSTs (GOGA). These results need to be compared with other model simulations with SST forcing in different ocean domains. In particular, we plan to study the relative importance of the tropical Pacific and South Atlantic Oceans on the SACZ variability by conducting two complementary experiments with SST forcing only in the tropical Pacific, or only in the South Atlantic. This experiment design should allow us to better isolate the remote Pacific forcing from the local Atlantic forcing. Results can then be compared with the results reported in this study.

Acknowledgments. We would like to acknowledge the contribution of Jeff Lee, who carried out the AGCM integrations at NCAR. We would also like to thank Dr. G.C. Hegerl for the helpful discussion about the signal-to-noise optimization analysis. Roberto Mechoso and an anonymous reviewer provided valuable comments on the manuscript. This work is supported by the NOAA's Global Climate Change Program under Grants NA06GP0423 and NA86GP0303.

REFERENCES

Aceituno, P., 1988: On the functioning of the Southern Oscillation in the South American sector. Part I: Surface climate. *Mon. Wea. Rev.,* **116,** 505–524.

Allen, M. R., and L. A. Smith, 1997: Optimal filtering in singular spectrum analysis. *Phys. Lett.,* **234,** 419–428.

Bladé, I., 1997: The influence of midlatitude ocean–atmosphere coupling on the low-frequency variability of a GCM. Part I: No tropical SST forcing. *J. Climate,* **10,** 2087–2106.

Chang, P., R. Saravanan, L. Ji, and G. C. Hegerl, 2000: The effect of local sea surface temperature on atmospheric circulation over the tropical sector. *J. Climate,* **13,** 2195–2216.

Cook, K. H., 2000: The South Indian convergence zone and interannual rainfall variability over southern Africa. *J. Climate,* **13,** 3789–3804.

Figueroa, S. N., P. Satyamurty, and P. L. Silva Dias, 1995: Simulations of the summer circulation over the South American region with an eta coordinate model. *J. Atmos. Sci.,* **52,** 1573–1584.

Hasselmann, K., 1979: On the signal-to-noise problem in atmospheric response studies. *Meteorology of the Tropical Oceans,* D. B. Shaw, Ed., Royal Meteorological Society, 251–259.

Hess, P. G., D. S. Battisti, and P. J. Rasch, 1993: Maintenance of the intertropical convergence zones and the large-scale tropical circulation on a water-covered earth. *J. Atmos. Sci.,* **50,** 691–713.

Hoskins, B. J., and D. J. Karoly, 1981: The steady linear response of a spherical atmosphere to thermal and orographic forcing. *J. Atmos. Sci.,* **38,** 1179–1196.

Kalnay, E., K. C. Mo, and J. Paegle, 1986: Large-amplitude, short-scale stationary Rossby waves in the Southern Hemisphere: Observations and mechanistic experiments to determine their origin. *J. Atmos. Sci.,* **43,** 252–275.

Kiladis, G. N., and K. M. Weickmann, 1992: Circulation anomalies associated with tropical convection during northern winter. *Mon. Wea. Rev.,* **120,** 1900–1923.

Kodama, Y.-M., 1992: Large-scale common features of subtropical convergence zones (the Baiu frontal zone, the SPCZ and the SACZ). Part I: Characteristics of subtropical frontal zones. *J. Meteor. Soc. Japan,* **70,** 813–836.

——, 1993: Large-scale common features of subtropical convergence zones (the Baiu frontal zone, the SPCZ, and the SACZ). Part II: Conditions of the circulations for generating the STCZs. *J. Meteor. Soc. Japan,* **71,** 581–610.

Lenters, J. D., and K. H. Cook, 1995: Simulation and diagnosis of the regional summertime precipitation climatology of South America. *J. Climate,* **8,** 2988–3005.

Matthews, A. J., and G. N. Kiladis, 1999: Interaction between ENSO, transient circulation, and tropical convection over the Pacific. *J. Climate,* **12,** 3062–3086.

North, G. R., T. L. Bell, R. F. Cahalan, and F. J. Moeng, 1982: Sampling errors in the estimation of empirical orthogonal functions. *Mon Wea. Rev.,* **110,** 699–706.

Peixoto, J. P., and A. H. Oort, 1992: *Physics of Climate.* American Institute of Physics, 520 pp.

Robertson, A. W., and C. Mechoso, 2000: Interannual and decadal variability of the South Atlantic convergence zone. *Mon. Wea. Rev.,* **128,** 2947–2957.

Saravanan, R., 1998: Atmospheric low-frequency variability and its relationship to midlatitude SST variability: Studies using the NCAR Climate System Model. *J. Climate,* **11,** 1386–1404.

——, and P. Chang, 2000: Interaction between tropical Atlantic variability and El Niño–Southern Oscillation. *J. Climate,* **13,** 2177–2194.

Venegas, S. A., L. A. Mysak, and N. Straub, 1997: Atmosphere–ocean coupled variability in the South Atlantic. *J. Climate,* **10,** 2904–2920.

Venzke, S., M. R. Allen, R. T. Sutton, and D. P. Rowell, 1999: The atmospheric response over the North Atlantic to decadal changes in sea surface temperature. *J. Climate,* **12,** 2562–2584.

Wang, B., and T. Li, 1993: A simple model of relevance to short-term climate variations. *J. Atmos. Sci.,* **50,** 260–284.